robotics

MDPI

Finite-Time State Estimation for an Inverted Pendulum under Input-Multiplicative Uncertainty

Anu Kossery Jayaprakash [1,*], Krishna Bhavithavya Kidambi [2], William MacKunis [1], Sergey V. Drakunov [1] and Mahmut Reyhanoglu [3]

[1] Department of Physical Sciences, Embry-Riddle Aeronautical University, Daytona Beach, FL 32114, USA; mackuniw@erau.edu (W.M.); drakunov@erau.edu (S.V.D.)

[2] Institute for Systems Research, University of Maryland, College Park, MD 2074, USA; kidambi@umd.edu

[3] NC State-UNC Asheville Joint Engineering Programs, Asheville, NC 28804, USA; mreyhan@ncsu.edu

* Correspondence: kosserya@my.erau.edu

check for updates

Abstract: A sliding mode observer is presented, which is rigorously proven to achieve finite-time state estimation of a dual-parallel underactuated (i.e., single-input multi-output) cart inverted pendulum system in the presence of parametric uncertainty. A salient feature of the proposed sliding mode observer design is that a rigorous analysis is provided, which proves finite-time estimation of the complete system state in the presence of input-multiplicative parametric uncertainty. The performance of the proposed observer design is demonstrated through numerical case studies using both sliding mode control (SMC)- and linear quadratic regulator (LQR)-based closed-loop control systems. The main contribution presented here is the rigorous analysis of the finite-time state estimator under input-multiplicative parametric uncertainty in addition to a comparative numerical study that quantifies the performance improvement that is achieved by formally incorporating the proposed compensator for input-multiplicative parametric uncertainty in the observer. In summary, our results show performance improvements when applied to both SMC- and LQR-based control systems, with results that include a reduction in the root-mean square error of up to 39% in translational regulation control and a reduction of up to 29% in pendulum angular control.

1. Introduction

Stabilization control of an inverted pendulum is a widely addressed problem in the field of control system engineering. The dynamics of an inverted pendulum system have several inherent control design challenges, including sensor limitations, a high degree of nonlinearity, parameter variations, and unmodeled disturbances. Moreover, the inverted pendulum is a well-known example of an underactuated (i.e., single-input multi-output (SIMO)) system, which presents additional non-trivial theoretical challenges in the control design.

1.1. Motivation

A classical implementation example is the cart inverted pendulum shown in Figure 1, in which a DC motor drives a cart supporting a pendant-type pendulum. Numerous techniques have been proposed to control the cart inverted pendulum, including sliding mode control (SMC) [1–3], backstepping

SMC [4,5], super-twisting control [6,7], higher-order SMC [8,9], adaptive control [10], passivity-based control [11], energy-based control [12], linear quadratic regulator (LQR)-based control [13,14], fuzzy logic-, and neural network-based control [15–17], model-predictive control [18], optimal control [19] and others. A vibrational control strategy is presented in [20], where external vibrations are applied to optimize the working conditions in an experimental electro-mechanical system with uncertain dynamics. While several successful control methods have been presented in the research literature, there remain multiple open challenges to be addressed in nonlinear estimation and control system design for the inverted pendulum **under model uncertainty**. For reliable control of a cart inverted pendulum under realistic operating conditions, model uncertainty and parameter variations must be formally incorporated in the control design, especially for the case when the parametric uncertainty appears as multiplicative to the control input term.

1.2. Literature Survey

System linearization is a popular approach that is utilized to recast the inverted pendulum dynamics in a more tractable form [21–25]. In [22], a comparison study is provided between three linear control strategies: PID, LQR, and model predictive control (MPC). The MPC strategy in [22] is formulated as a constrained finite-time optimization problem, which is motivated by the desire to incorporate practical constraints on the control action and the states. The performance comparison is presented via experimental results in [22], which show similar pendulum rod angle stabilization performance between the three control methods over a small range of angular excursions. The results further show that the optimal LQR and MPC controllers were able to simultaneously stabilize the cart's horizontal motion as well as the pendulum angle. An optimal LQR strategy is also presented in [25], which employs particle swarm optimization to stabilize an inverted pendulum system while simultaneously determining the optimal LQR control under a finite-time duration of the cost function. To address the additional control challenges of limited sensing and actuation, the case study in [24] shows an optimal stabilizing controller for an inverted pendulum system with only one position sensor and one force actuator. The result in [24] is achieved by first choosing a reasonable sensor location by analyzing the effect of the sensor location on the system zeros. The controller is then designed, which is shown to effectively minimize the H_∞ norm of the Gang-of-Four transfer matrix.

The aforementioned linear approaches have clearly demonstrated promising performance in their respective control objectives. Stabilization schemes based on linearization about the unstable equilibrium point can limit the range of effectiveness of the control system, especially for highly nonlinear dynamic systems such as the inverted pendulum. Moreover, parameter variations and unmodeled disturbances are inevitable challenges that must be addressed for practical controller implementation.

To ensure reliable controller operation over a wide range of operating conditions, nonlinear estimation and control methods are often applied to the inverted pendulum regulation problem [6,26–30]. In [26], a continuous fixed-time convergent control algorithm is presented for regulation control of a cart inverted pendulum subject to unbounded disturbances. The control method in [26] guarantees a pre-established convergence time, which is insensitive to initial conditions and unbounded external disturbances. In [6], a super-twisting algorithm is proposed to control a cart-pole inverted pendulum system. The control strategy in [6] is motivated in part by the desire to improve chatter reduction above standard chatter attenuation approaches. To eliminate the need for direct velocity measurements, the control system in [6] employs a homogeneous sliding mode observer to estimate the velocities. The sliding mode observer is shown to achieve input-to-state (ISS) stability of the estimation errors in the presence of model uncertainties and external disturbances. The observer design in [6] assumes precise knowledge of the input gain matrix in the plant model.

The control of different variations of the inverted pendulum such as rotary inverted pendulum and wheeled inverted pendulum can be found in [31–35]. The control of a rotary inverted pendulum utilizing on–off-type cold gas thrusters as the actuators, which have high similarities with thruster actuated spacecrafts with slosh dynamics is detailed in [31]. A full-state feedback controller is designed in [31] based on a linear model of the rotary inverted pendulum. The result in [32] describes a time-optimal control method for a wheeled inverted pendulum vehicle applied to specified trajectories. The controller in [32] is implemented using a trajectory tracking controller considering a linear model of WIP. The article in [33] presents the design and the experimental validation of a novel 3-degree-of-freedom (DOF) pendulum-like cable-driven robot capable of executing point-to-point motions by leveraging partial feedback linearization control and on-line trajectory planning based on adaptive frequency oscillators (AFOs). A diffeomorphism technique is used in [33] to remodel the nonlinear plant model. All of the aforementioned studies have demonstrated good results with respect to their control objectives. However, the contribution of the current result focuses on finite-time state estimation of a dual-parallel underactuated inverted pendulum system in the presence of input-multiplicative parametric uncertainty in the dynamic model. The current result is motivated by practical implementation scenarios where only position encoders are available for feedback measurements.

1.3. Contribution

The nonlinear inverted pendulum control techniques summarized in Section 1.2 have been shown to be effective in achieving their respective control objectives. However, these examples require fairly precise knowledge of the dynamic model and/or the actuator model, which might be difficult to obtain in practice due to parameter variations and unmodeled nonlinearities, for example.

In this paper, a sliding mode observer (SMO) is presented, which is rigorously proven to achieve finite-time state estimation for a dual-parallel underactuated cart inverted pendulum system in the presence of parametric uncertainty. The observer design is fundamentally motivated by practical implementation considerations, where only position encoders are available for feedback measurements. A salient feature of the proposed sliding mode observer design is that a rigorous analysis is provided, which proves that finite-time estimation of the complete system state can be achieved in the presence of input-multiplicative parametric uncertainty. Specifically, based on the assumption of partial knowledge of the system parameters, a set of gain conditions is derived, within which finite-time state estimation can be proved. As a proof-of-concept, the proposed observer is applied to closed-loop control systems using both SMC and LQR controllers. To demonstrate the performance of the proposed sliding mode estimation strategy, a comparative numerical simulation study is provided, which demonstrates the performance of the proposed observer design when applied to closed-loop systems using both LQR and standard SMC. The numerical comparison study clearly shows the performance improvement that can be achieved by formally incorporating the input uncertainty compensator in the observer.

The major contributions of this paper are as follows:

1. An SMO design is proposed for a dual-parallel underactuated system, which is shown to achieve finite-time state estimation in the presence of input-multiplicative parametric uncertainty.
2. Detailed numerical comparison study of the proposed SMO as part of closed-loop control systems using LQR and SMC, which clearly demonstrate a significant performance improvement is achieved using the proposed SMO with uncertainty compensation element.
3. Detailed numerical data quantifying the performance improvement achieved using the proposed SMO under conditions with up to 20% parameter deviations. Numerical results were obtained under ten randomized iterations of parameter deviations.

1.4. Organization of the Manuscript

This paper is organized as follows: Section 2 presents the mathematical model of the inverted cart pendulum and the model properties. The proposed SMO design is detailed in Section 3. Section 4 details the sliding mode control law utilized as a proof-of-concept and the stability analysis is summarized in Section 5. The results obtained in the simulation are presented in Section 6. In the last section, the conclusions are presented along with a summary of future work.

2. Dynamic Model and Properties

In this section, the dynamic model of the inverted pendulum is described, and the model is re-cast in a form amenable to observer design with input uncertainty compensation. To facilitate the subsequent observer design and analysis, a list of symbols is provided below.

2.1. List of Symbols

M_c : Mass of the cart	$\theta(t)$	: Angular displacement
m : Mass of the pendulum bob	$F(t)$	: Control force applied to the pivot.
l : Rod length	$k_1, k_2, k_3, k_4, Z_0, \lambda, \epsilon$	: Control gains
$h(t)$: Horizontal displacement	$m_{11}, m_{12}, \beta_{1,1}, \beta_{1,2}, \beta_{2,1}, \beta_{2,2}$: Observer gains

2.2. Inverted Pendulum Dynamics

The dynamic model of the inverted cart pendulum shown in Figure 1 can be expressed as [36]

$$\ddot{h} = \frac{F - mg\cos\theta\sin\theta + ml\dot{\theta}^2\sin\theta}{M_c + m\sin^2\theta} \tag{1}$$

$$\ddot{\theta} = \frac{(M_c + m)g\sin\theta - F\cos\theta - ml\dot{\theta}^2\sin\theta\cos\theta}{M_c l + ml\sin^2\theta} \tag{2}$$

where $M_c \in \mathbb{R}^+$ is the mass of the cart, $m \in \mathbb{R}^+$ is the mass of the pendulum bob, $l \in \mathbb{R}^+$ is the rod length, $\theta(t) \in \mathbb{R}$ is the angular displacement from the vertical axis, $h(t) \in \mathbb{R}$ is the horizontal displacement, and $F(t) \in \mathbb{R}$ is the control force applied to the pivot in the horizontal direction.
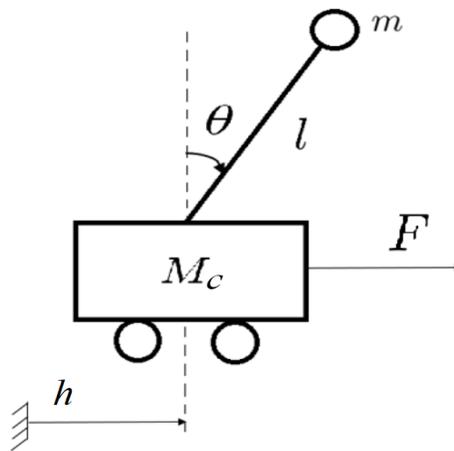

Figure 1. Diagram of the cart inverted pendulum.

The dynamic model can be expressed in state form by defining states as $x_1(t) = h(t)$, $x_2(t) = \theta(t)$, $x_3(t) = \dot{h}(t)$, $x_4(t) = \dot{\theta}(t)$, which results in a set of first-order ODEs given by

$$\dot{x}_1 = x_3 \tag{3}$$

$$\dot{x}_2 = x_4 \tag{4}$$

$$\dot{x}_3 = \frac{F - mg\cos x_2 \sin x_2 + mlx_4^2 \sin x_2}{M_c + m\sin^2 x_2} \tag{5}$$

$$\dot{x}_4 = \frac{(M_c + m)g\sin x_2 - F\cos x_2 - mlx_4^2 \sin x_2 \cos x_2}{M_c l + ml\sin^2 x_2} \tag{6}$$

$$y = \begin{bmatrix} x_1 & x_2 \end{bmatrix}^T. \tag{7}$$

where $y(t) \in \mathbb{R}^2$ denotes the output vector (i.e., only position encoder measurements are available for feedback).

The state equations in (3)–(7) can be expressed in compact form as

$$\dot{x} = f(x) + g(x)u \tag{8}$$

$$y = Cx \tag{9}$$

where, $x = \begin{bmatrix} x_1 & x_2 & x_3 & x_4 \end{bmatrix}^T \in \mathbb{R}^4$, and

$$C \triangleq \begin{bmatrix} 1 & 0 & 0 & 0 \\ 0 & 1 & 0 & 0 \end{bmatrix}$$

and the nonlinear function $f(x) \in \mathbb{R}^4$ is explicitly defined as

$$f(x) \triangleq \begin{bmatrix} x_3 \\ x_4 \\ \frac{-mg\cos x_2 \sin x_2 + mlx_4^2 \sin x_2}{M_c + m\sin^2 x_2} \\ \frac{(M_c + m)g\sin x_2 - mlx_4^2 \sin x_2 \cos x_2}{M_c l + ml\sin^2 x_2} \end{bmatrix} \tag{10}$$

In Equation (8), $u(t) \triangleq F(t)$ to standardize notation. To simplify the notation in the subsequent estimation error convergence, auxiliary functions will be defined as

$$f_1(x) \triangleq \begin{bmatrix} x_3 \\ x_4 \end{bmatrix} \tag{11}$$

$$f_2(x) \triangleq \begin{bmatrix} \frac{-mg\cos x_2 \sin x_2 + mlx_4^2 \sin x_2}{M_c + m\sin^2 x_2} \\ \frac{(M_c + m)g\sin x_2 - mlx_4^2 \sin x_2 \cos x_2}{M_c l + ml\sin^2 x_2} \end{bmatrix} \tag{12}$$

In the presence of parametric uncertainty in the dynamic model, the input matrix $f(x)$ can be decomposed as the sum of a known, nominal matrix $f_0(x) \in \mathbb{R}^4$ and an uncertain offset matrix $f_\Delta(x) \in \mathbb{R}^4$ as

$$f(x) = f_0(x) + f_\Delta(x) \tag{13}$$

Then,

$$f_1(x) = f_{10}(x) \tag{14}$$

$$f_2(x) = f_{20}(x) + f_{2\Delta}(x) \tag{15}$$

Note that the equality in Equation (14) simply indicates that there is no parametric uncertainty in $f_1(x)$. The nonlinear function $g(x) \in \mathbb{R}^4$ is explicitly defined as

$$g(x) \triangleq \begin{bmatrix} g_1(x) \\ g_2(x) \end{bmatrix} \tag{16}$$

where,

$$g_1(x) \triangleq \begin{bmatrix} 0 \\ 0 \end{bmatrix} \tag{17}$$

$$g_2(x) \triangleq \begin{bmatrix} \frac{1}{M_c + m \sin^2 x_2} \\ -\frac{\cos x_2}{M_c l + ml \sin^2 x_2} \end{bmatrix} \tag{18}$$

Similarly, as in Equation (13), the input gain matrix $g(x)$ can be decomposed as the sum of a known, nominal matrix $g_0(x) \in \mathbb{R}^4$ and an uncertain offset matrix $g_\Delta(x) \in \mathbb{R}^4$ as

$$g(x) = g_0(x) + g_\Delta(x). \tag{19}$$

Then,

$$g_1(x) = g_{10}(x) \tag{20}$$

$$g_2(x) = g_{20}(x) + g_{2\Delta}(x) \tag{21}$$

By substituting Equations (13) and (19) into Equation (8), the dynamic model can be rewritten as

$$\dot{x} = f_0(x) + f_\Delta(x) + g_0(x)u + g_\Delta(x)u. \tag{22}$$

Property 1. *Based on the definitions in Equations (7)–(16), it follows that the first and second partial derivatives of $f(x), g(x),$ and $y(t)$ with respect to $x(t)$ exist and are bounded, provided $x(t)$ is bounded.*

Property 2. *The denominators of the expressions in $f_2(x)$ and $g_2(x)$ in Equations (12) and (18) remain positive for all $x(t) \in R^4$, so the open loop dynamics remain singularity-free for all $x(t) \in R^4$.*

Assumption 1. *The initial condition for the state $x(t)$ lies in the bounded region $x(0) \in X_0 \subset \mathbb{R}^4$.*

3. Observer Design

In this section, an observer design is presented, which estimates the full state $x(t)$ of the uncertain system described in Equation (22) using only the measurable output $y(t)$. The analysis presented here provides the detailed derivation of observer gain conditions under which a sliding mode estimator can be proven to achieve finite-time state estimation in the presence of parametric uncertainty in the input gain matrix in Equation (8).

To facilitate the following estimator design and convergence analysis, the state vector $x(t)$ will be decomposed as

$$x(t) = \begin{bmatrix} X_1^T(t) & X_2^T(t) \end{bmatrix}^T \tag{23}$$

where $X_1(t) \triangleq \begin{bmatrix} x_1(t) & x_2(t) \end{bmatrix}^T \in \mathbb{R}^2$ and $X_2(t) \triangleq \begin{bmatrix} x_3(t) & x_4(t) \end{bmatrix}^T \in \mathbb{R}^2$.

Based on these definitions,

$$\dot{X}_1 = f_1(x) = X_2 \tag{24}$$

$$\dot{X}_2 = f_2(x) + g_2(x)u \tag{25}$$

In the following observer design and analysis, the $sgn(*)$ operation is taken component-wise on the vector argument; and $|*|$ denotes the standard 1-norm. The sliding mode observer that estimates the full state $x(t)$ for the uncertain cart inverted pendulum dynamic system in Equation (8) can be designed as

$$\dot{\hat{x}} = M(\hat{x}, u)sgn\big(\Psi(t) - \hat{x}(t)\big) + f_0(\hat{x}) + g_0(\hat{x})u(t) \tag{26}$$

where $\hat{x}(t) = \begin{bmatrix} \hat{X}_1^T(t) & \hat{X}_2^T(t) \end{bmatrix}^T \in \mathbb{R}^4$ denotes the estimate of $x(t)$, $f_0(\cdot)$ is introduced in Equation (13), $g_0(\cdot)$ is introduced in Equation (19), and $M(\hat{x}, u) \in \mathbb{R}^{4 \times 4}$ denotes a positive definite, diagonal sliding gain term, which can be expressed as

$$M(\hat{x}, u) = \text{diag}\left[m_1(\hat{x}), m_2(\hat{x}, u)\right] \tag{27}$$

where $m_1(\hat{x})$, $m_2(\hat{x}, u) \in \mathbb{R}^{2 \times 2}$, denote subsequently designed sliding gain terms, and $diag(\cdot)$ denotes a diagonal matrix containing the vector argument.

To facilitate the subsequent convergence analysis, the control gains $m_1(\hat{x})$ and $m_2(\hat{x})$ are designed to satisfy the inequalities.

$$m_1 > \sup_{x \in X_0} \|X_2(t)\| \tag{28}$$

$$m_2(\hat{x}, u) = \begin{bmatrix} \beta_{1,1} & 0 \\ 0 & \beta_{2,1} \end{bmatrix} + \begin{bmatrix} \beta_{1,2}|u| & 0 \\ 0 & \beta_{2,2}|u| \end{bmatrix} \tag{29}$$

where the auxiliary gain terms $\beta_{i,j}$, for $i, j = 1, 2$ are selected to satisfy

$$\min\{\beta_{1,1}, \beta_{2,1}\} > \sup_{x \in X_0} \|f_{20}(x) - f_{20}(\hat{x}) + f_{2\Delta}(x)\|_\infty \tag{30}$$

$$\min\{\beta_{1,2}, \beta_{2,2}\} > \sup_{x \in X_0} \|g_{20}(x) - g_{20}(\hat{x}) + g_{2\Delta}(x)\|_\infty \tag{31}$$

Additionally in Equation (26), $\Psi(t) = [\psi_1^T(t), \psi_2^T(t)]^T \in \mathbb{R}^4$ is defined via the modified recursive form [37].

$$\psi_1(t) = X_1(t) \tag{32}$$

$$\psi_2(t) = m_1(\hat{x})\Big\{sgn\big(X_1(t) - \hat{X}_1(t)\big)\Big\}_{eq} \tag{33}$$

where, $\{sgn(\cdot)\}_{eq}$ denotes a continuous "equivalent value operator" of the discontinuous signum function [38], which can be obtained via low-pass filtering of the signum function.

Note that the observer equations for $\dot{\hat{X}}_1(t)$ will not include $u(t)$, whereas the equations for $\dot{\hat{X}}_2(t)$ include $u(t)$ based on Equations (16) and (19).

$$\dot{\hat{X}}_1 = m_1(\hat{x})sgn\left(\psi_1(t) - \hat{X}_1(t)\right) \tag{34}$$

$$\dot{\hat{X}}_2 = m_2(\hat{x}, u)sgn\left(\psi_2(t) - \hat{X}_2(t)\right) + f_{20}(\hat{x}) + g_{20}(\hat{x})u(\hat{x}) \tag{35}$$

By designing the observer gain matrix $M(\hat{x}, u)$ according to the sufficient conditions in inequalities Equations (26)–(31), it will be shown that the sliding mode observer in Equation (26) achieves finite-time estimation of the state $x(t)$ using only measurements of the output signal $y(t)$.

Remark 1. *(**Observer Gain Matrix** $M(\hat{x}, u)$) The observer gain matrix $M(\cdot)$ introduced in Equation (26) can include the state estimate $\hat{x}(t)$ in general. However, this is not a requirement; and the subsequent estimator convergence proof can be carried out for the case where $M(\cdot)$ depends only on the measurable control input $u(t)$ and constant observer gains, provided Property 1 and Assumption 1 are satisfied.*

Remark 2. *(**Observer Gain Selection**) Based on the boundedness of the initial condition set X_0 (see Assumption 1), the observer gain matrix M can be selected to ensure that $\hat{x}(t) = x(t)$ after some finite time t_1, where t_1 can be made arbitrarily small.*

Assumption 2. *The initial estimation errors are bounded such that:*

$$\tilde{X}_1(0) = X_1(0) - \hat{X}_1(0) < \varepsilon_1 \tag{36}$$

$$\tilde{X}_2(0) = X_2(0) - \hat{X}_2(0) < \varepsilon_2 \tag{37}$$

where $\varepsilon_1 \in \mathbb{R}^+$ and $\varepsilon_2 \in \mathbb{R}^+$ are known bounding constants.

Preliminary results show that Assumption 2 is mild in the sense that the proposed estimation and control method performs well over a wide range of parametric uncertainty in the $f(x)$ and $g(x)$ matrices.

Theorem 1. *Provided Assumption 2 is satisfied, the sliding mode observer in Equation (26) assures that the states and estimates remain bounded, and that finite-time estimation of the state $x(t)$ is achieved in the sense that $\hat{x}(t) \equiv x(t)$ for $t \geq t_1$, where $t_1 < \infty$.*

Proof. The estimation error can be defined as

$$\tilde{x}(t) \triangleq x(t) - \hat{x}(t). \tag{38}$$

The estimation error dynamics can be obtained by taking the time derivative of Equation (38) as

$$\dot{\tilde{x}}(t) = \dot{x}(t) - \dot{\hat{x}}(t). \tag{39}$$

By utilizing Equations (22), (23), (26) and (27), the estimation error dynamics for $\tilde{X}_1(t)$ and $\tilde{X}_2(t)$ can be expressed as

$$\dot{\tilde{X}}_1(t) = X_2(t) - m_1(\hat{x})sgn\left(X_1(t) - \hat{X}_1(t)\right) \tag{40}$$

$$\dot{\tilde{X}}_2(t) = f_{20}(x) - f_{20}(\hat{x}) + \left[g_{20}(x) - g_{20}(\hat{x})\right]u(\hat{x}) \tag{41}$$
$$+ f_{2\Delta}(x) + g_{2\Delta}(x)u(\hat{x}) - m_2(\hat{x}, u)sgn\left(\psi_2(t) - \hat{X}_2(t)\right)$$

where $g_{20}(x) \in \mathbb{R}^2$ is defined in Equation (21).

By using inequality Equation (28) in Equation (40), the following inequality can be obtained:

$$\dot{\tilde{X}}_1 \leq -\kappa_1 sgn\left(\tilde{X}_1\right). \tag{42}$$

where $\kappa_1 \in \mathbb{R}^+$ is a known bounding constant.

The differential inequality in Equation (42) can be solved to obtain

$$|\tilde{X}_1(t)| \leq |\tilde{X}_1(0)| - \kappa_1 t. \tag{43}$$

Thus, from Equation (43),
$$\tilde{X}_1(t) = 0 \text{ for } t \geq t_0 \tag{44}$$

where t_0 is a calculable time instant. Hence, $\hat{X}_1(t) = X_1(t)$ for $t \geq t_0$.

Given that $\tilde{X}_1(t) = 0$ for $t \geq t_0$, $\dot{\tilde{X}}_1(t) = 0$; and Equation (40) can be used to obtain

$$X_2(t) = m_1(\hat{x})sgn\left(X_1(t) - \hat{X}_1(t)\right) \tag{45}$$

for $t \geq t_0$. Thus, $\psi_2(t) = X_2(t)$ from Equation (33); and Equations (26) and (41) can be used to obtain

$$\dot{\tilde{X}}_2(t) = f_{20}(x) - f_{20}(\hat{x}) + \left[g_{20}(x) - g_{20}(\hat{x})\right]u(\hat{x}) \tag{46}$$
$$+ f_{2\Delta}(x) + g_{2\Delta}(x)u(\hat{x}) - m_2(\hat{x}, u)sgn\left(X_2(t) - \hat{X}_2(t)\right)$$

Note that, based on Assumption 2, the observer gains $\beta_{i,j}$, for $i, j = 1, 2$ can be selected to achieve finite-time state estimation using only approximate knowledge of the system parameters. Provided inequalities Equations (30), (31) (36) and (37) are satisfied, the solution to Equation (46) can be upper bounded as

$$\dot{\tilde{X}}_2(t) \leq -\kappa_2 sgn(\tilde{X}_2(t)) \Rightarrow \tag{47}$$
$$|\tilde{X}_2(t)| \leq |\tilde{X}_2(0)| - \kappa_2 t \tag{48}$$

where $\kappa_2 \in \mathbb{R}^+$ is a known bounding constant. Since $|\tilde{X}_2(t)| \geq 0$, further, inequality Equation (48) can be used to prove that $X_2(t)$ remains bounded throughout observer operation, provided Assumption 1 is satisfied. Proof of Equation (48) can be found in [39] and is omitted here for brevity. □

Remark 3. *(Input Uncertainty Compensation) Note that, based on the design of the observer gain m_2 in Equation (29), the auxiliary observer gains $\beta_{1,2}$ and $\beta_{2,2}$ serve the specific purpose of compensating for the input-multiplicative parametric uncertainty present in $g(x)$. Thus, for non-zero values of $\beta_{1,2}$ and $\beta_{2,2}$, the observer includes input uncertainty compensation; and zero values of $\beta_{1,2}$ and $\beta_{2,2}$ represent no input uncertainty*

compensation in the observer. The subsequent simulation results will use this fact to present comparative results that clearly demonstrate the performance improvement that is attained by employing the input uncertainty compensator in the observer design.

Figure 2 shows the block diagram of the proposed sliding mode observer and controller system. The sliding mode controller illustrated here, is detailed in the Section 4.
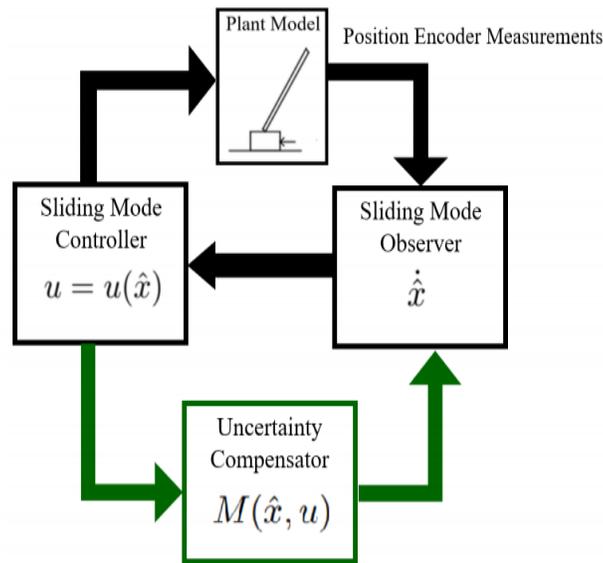

Figure 2. High level schematic overview of the proposed sliding mode observer and controller system.

4. Control Development

To demonstrate the practical applicability of the proposed sliding mode observer, the observer will be employed in closed-loop control systems using two different control methods: sliding mode control and LQR control. For completeness in describing the sliding mode control design tested in the subsequent simulation results, this section summarizes the structure of the sliding mode control method and the sliding surface design; both of which are motivated by the objective of stabilizing ($h = 0$ and $\theta = 0$) the SIMO inverted pendulum system described by Equations (8) and (9).

4.1. Sliding Mode Controller

To achieve the aforementioned control objective, the observer will be applied to a sliding mode control law with a periodic switching function defined as [40].

$$u(t) = Z_0 \ sgn\left\{ \sin\left[\frac{\pi}{\epsilon}\left(s(\hat{x}(t)) + \lambda \int_0^t \tanh\left(s(\hat{x}(\tau))\right)d\tau \right)\right]\right\} \tag{49}$$

where Z_0, λ, $\epsilon \in \mathbb{R}$ are control parameters. In Equation (49), $s(\hat{x}(t)) = 0$ is a sliding surface and $s(\hat{x}(t)) \in \mathbb{R}$ is the sliding variable, which is defined based on the state model in Equations (3)–(6) as

$$s(\hat{x}(t)) = \frac{1}{2}(k_1\hat{x}_1 + k_3\hat{x}_3)^2 + \frac{1}{2}(k_2\hat{x}_2 + k_4\hat{x}_4)^2 \tag{50}$$

where k_1, k_2, k_3, $k_4 \in \mathbb{R}$ are positive, constant control gains. Note that $s(\hat{x}(t)) \to 0 \Rightarrow s(x(t)) \to 0 \Rightarrow \|x(t)\| \to 0$ for $t >= t_1$ based on Theorem 1.

Remark 4. (*Engineering design trade-off using SMC*) *From a control design perspective, standard sliding mode control (SMC) is a widely used technique for compensating for model uncertainty and bounded disturbances; however, chattering is a well-known drawback that is inherent in standard SMC. Note that the reduction of chattering is a subject of future work and is not the focus of the current result.*

5. Stability Analysis

Theorem 2. *The sliding mode control law in Equation (49) drives the system in Equations (8)–(16) to the sliding manifold $\mathcal{M} \triangleq \{x(t) : s(x) = 0\}$ in finite time provided the sufficient controllability condition*

$$\frac{\partial s(\hat{x})}{\partial \hat{x}} g(\hat{x}) \neq 0 \tag{51}$$

is satisfied for $t \geq 0$ and $\hat{x}(t) \in \mathbb{R}^n$, and where the control gain terms Z_0 and λ are selected to satisfy the bounding condition

$$\left| \frac{\partial s(\hat{x})}{\partial \hat{x}} g(\hat{x}) Z_0 \right| > \left| \frac{\partial s(\hat{x})}{\partial \hat{x}} f(\hat{x}) \right| + \lambda + \delta \tag{52}$$

for some $\delta > 0$.

Proof. Proof of Theorem 2 can be found in [40] and is omitted here to avoid distraction from the main result of the current work. □

Remark 5. *Inequality Equation (52) does not necessarily need to be fulfilled globally for all $\hat{x}(t)$ and t, but only in the bounded neighborhood which contains the trajectory. It can be guaranteed that all closed-loop trajectories remain in a bounded neighborhood, under the standard assumption that the upper bound on the initial condition set is known (see related Assumptions 1 and 2).*

Remark 6. (*Controllability Condition*) *It should be noted that the controllability condition in Equation (51) is a sufficient, not necessary, condition to ensure that the system remains controllable throughout closed-loop operation. The subsequent simulation results show that the control objective is achieved even in instances where Equation (51) is temporarily violated.*

Remark 7. *In the subsequent simulation section, the discontinuous signum function is approximated using a hyperbolic tangent (tanh) function, which is shown to achieve estimator and controller convergence of the discretized simulation model.*

6. Simulation Results

A detailed numerical simulation was created using Matlab/Simulink to demonstrate the performance of the proposed observer/control system. The details of the simulation software are summarized in Table 1. The simulation is based on the state space equations given in Equations (3)–(7), where the nominal values for the physical parameters of the inverted pendulum plant model are summarized in Table 2. The sliding mode observer is designed based on Equations (26)–(33), where the observer gains are selected as summarized in Table 3. The control gains were selected manually to achieve the desired response. Specifically, the control gains were tuned to achieve the best possible trade-off between regulation/tracking accuracy and control effort required.

Table 1. Software details.

Software	Version	Settings	
		Simulation/Model configuration Parameters / Solver Options	
MATLAB/Simulink	R2017b	Type	: Fixed step
		Solver	: ode4 (Runge-Kutta)
		Fixed step size	: 0.001

Table 2. Nominal parameter values.

$$M_c = 3.5 \text{ kg}$$
$$m = 0.32 \text{ kg}$$
$$l = 0.44 \text{ m}$$
$$g = -9.8 \text{ m/s}^2$$

Table 3. Observer gains.

Gain	*LQR*	*SMC*
m_{11}	2	2
m_{12}	2	2
$\beta_{1,1}$	0.01	0.02
$\beta_{1,2}$	1.9	0.05
$\beta_{2,1}$	0.1	0.1
$\beta_{2,2}$	0.5	0.5

By leveraging the previous discussion in Remark 3, the simulation shows a comparison study of control system performance **with input uncertainty compensation** in the estimator design against the performance **without the input uncertainty compensation** for three different scenarios: (1) LQR regulation control, (2) sliding mode regulation control, and (3) sliding mode trajectory tracking control. To provide a realistic demonstration of the closed-loop system performance under parametric uncertainty, each control system was simulated for 10 iterations of randomized parametric uncertainty in the plant model (i.e., using the Matlab rand function). Each scenario was tested over six different levels of randomized uncertainty: 5%, 7%, 10%, 15%, 18%, 20% (i.e., x% uncertainty means $m_{unc} = m \pm x$%). The average mean squared error (MSE) over the 10 iterations was then calculated for each of the six levels of uncertainty for the two cases: (1) estimator with compensation and (2) estimator without compensation.

6.1. Regulation Control Using LQR and SMC

The proposed observer was tested in closed-loop regulation control systems using both LQR and SMC controllers. To illustrate the performance of the observer in the presence of parametric uncertainty, Figures 3 and 4 show Monte Carlo-type results of 10 randomized iterations for the closed-loop LQR and SMC control systems, respectively, with and without the input uncertainty compensator in the observer. The example LQR results in Figure 3 were obtained using the weighting matrices Q = [100 0 0 0; 0 5 0 0; 0 0 100 0; 0 0 0 5]; and R = 2. Similar LQR results were obtained using various other selections of weighting matrices and were omitted here to adhere to page constraints. To summarize the results over six levels of parametric uncertainty, a bar graph of the average MSE is shown in Figure 5 and the corresponding MSE and RMS values are given in Table 4. The results in Figure 5 clearly show the improvement that is achieved using the observer with the uncertainty compensator in both the LQR and SMC systems. Figures 6 and 7 show the time evolution of the estimation error over the entire simulation time. Figure 8

shows the time evolution of the control input during closed-loop operation. Please note that the focus of the current result is on reliable finite-time estimation under parametric uncertainty, and chattering in SMC was not addressed.
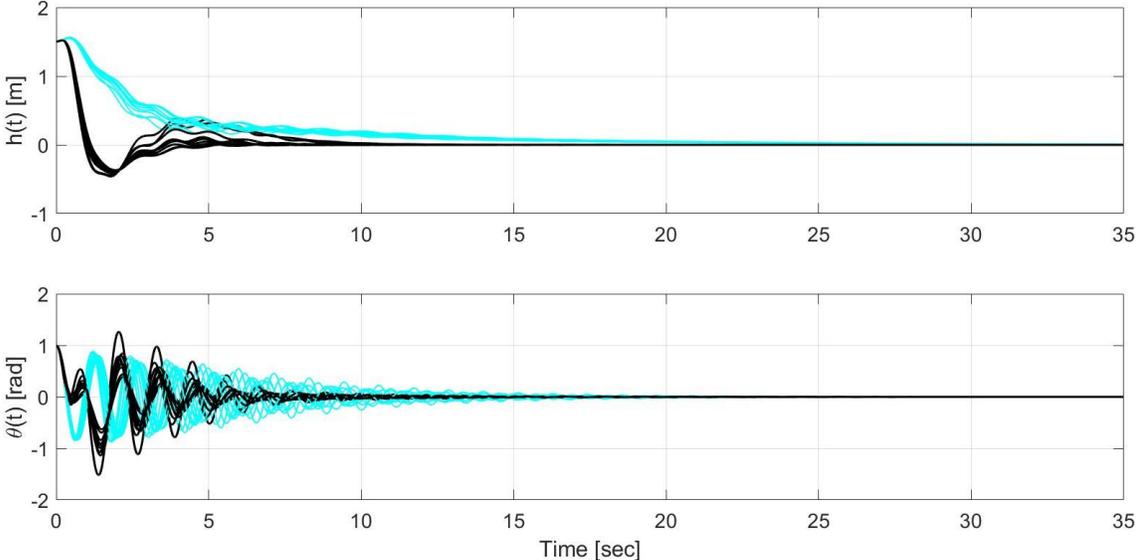

Figure 3. Time evolution of the state $h(t)$ and $\theta(t)$ for linear quadratic regulator (LQR) without uncertainty compensation (cyan) and LQR with uncertainty compensation (black) during closed-loop operation.
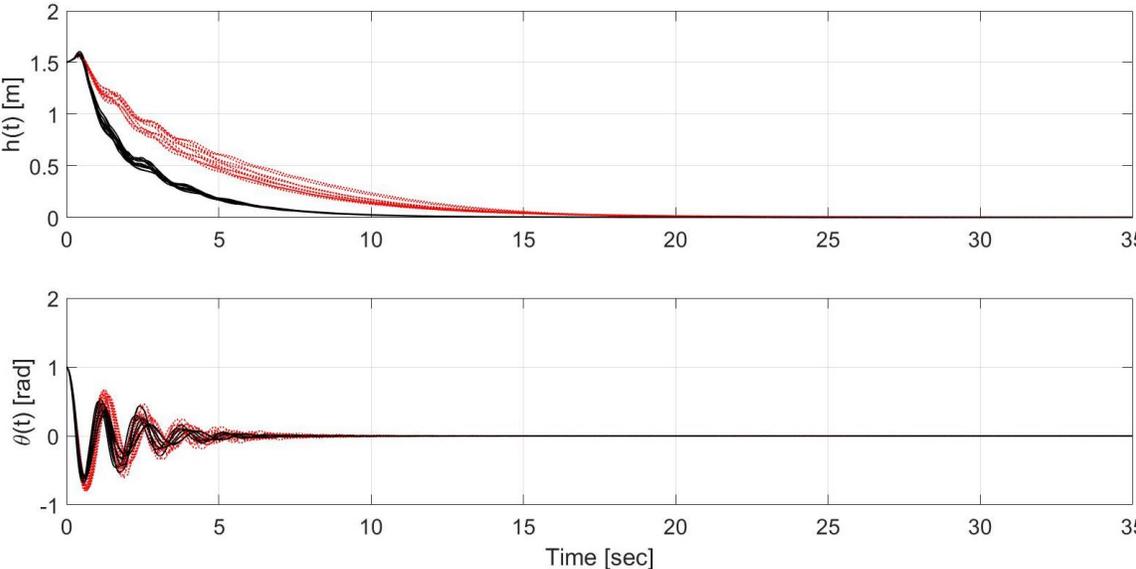

Figure 4. Time evolution of the state $h(t)$ and $\theta(t)$ for sliding mode control (SMC) without uncertainty compensation (red) and SMC with uncertainty compensation (black) during closed-loop operation.
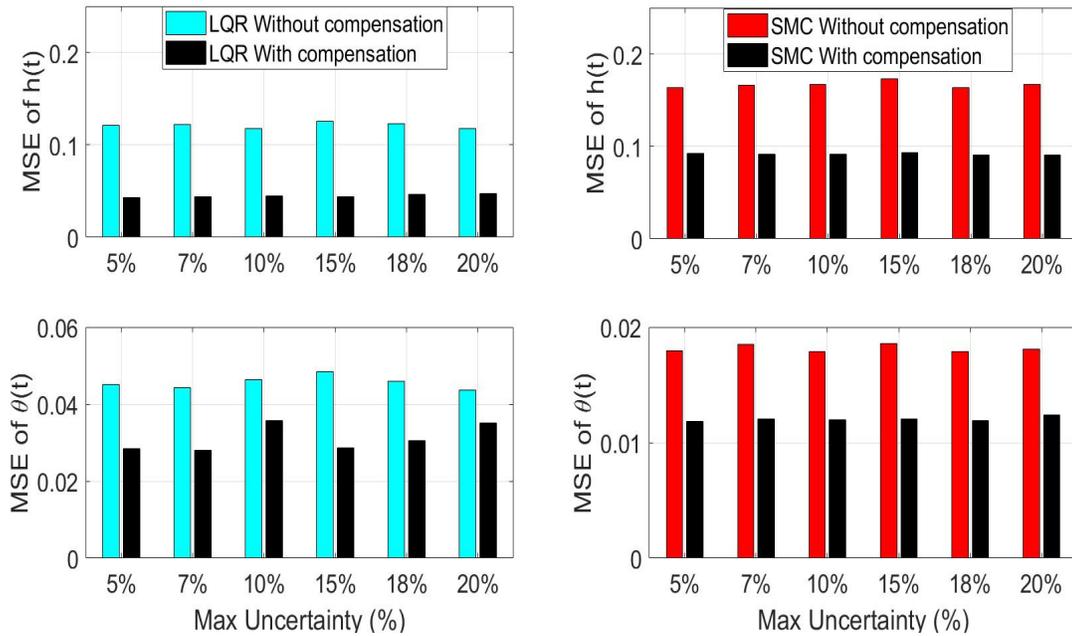
Figure 5. Average mean squared error (MSE) during closed-loop operation for 10 iterations of randomized parameter uncertainty using LQR (**left**) and SMC (**right**) with and without uncertainty compensation.
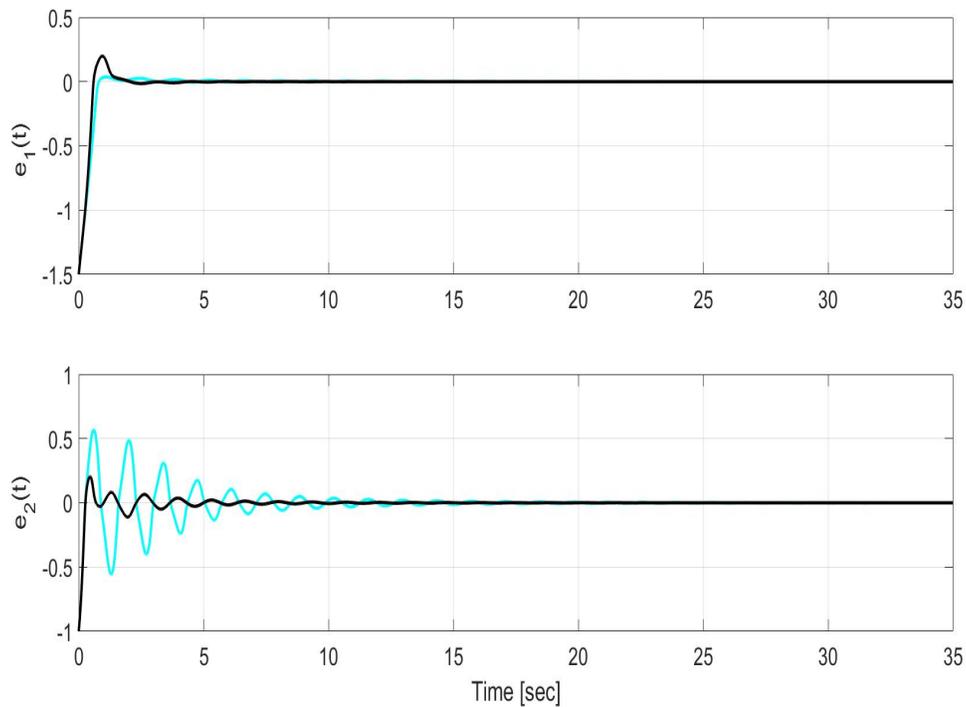

Figure 6. Time evolution of the estimation error in states $h(t)$ (**top**) and $\theta(t)$ (**bottom**) for LQR without uncertainty compensation (cyan) and LQR with uncertainty compensation (black) over the entire simulation time.
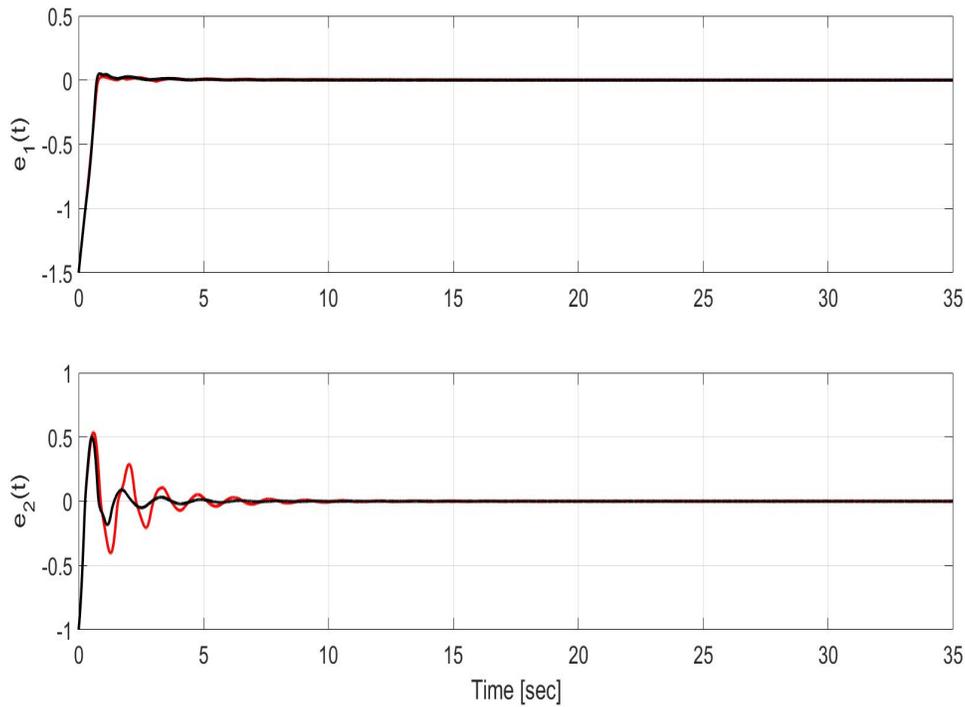
Figure 7. Time evolution of the estimation error in states $h(t)$ (**top**) and $\theta(t)$ (**bottom**) for SMC without uncertainty compensation (red) and SMC with uncertainty compensation (black) over the entire simulation time.

Table 4. Mean squared error (MSE) and root mean squared error (RMS) during closed-loop operation for 10 iterations of randomized parameter uncertainty using LQR and SMC (Regulation) with uncertainty compensation (**With C**) and without uncertainty compensation (**W/o C**).

| LQR REGULATION								
Unc	MSE of $h(t)$		MSE of $\theta(t)$		RMS of $h(t)$		RMS of $\theta(t)$	
(%)	W/o C	With C	W/o C	With C	W/o C	With C	W/o C	With C
5	0.1214	0.0432	0.04516	0.02842	0.3484	0.2078	0.2125	0.1686
7	0.1216	0.0436	0.04435	0.02798	0.3487	0.2088	0.2106	0.1673
10	0.1175	0.04448	0.04632	0.03572	0.3428	0.2109	0.2152	0.1890
15	0.125	0.04392	0.04838	0.02856	0.3536	0.2096	0.2200	0.1690
18	0.1227	0.04655	0.04595	0.0306	0.3503	0.2158	0.2144	0.1749
20	0.1178	0.04754	0.04362	0.03506	0.3432	0.2180	0.2089	0.1872
Average	0.121	0.044882	0.04563	0.031057	0.34783	0.21182	0.213582	0.176003
Reduction (%)	62.91		31.94		39.10		17.59	
SMC REGULATION								
Unc	MSE of $h(t)$		MSE of $\theta(t)$		RMS of $h(t)$		RMS of $\theta(t)$	
(%)	W/o C	With C	W/o C	With C	W/o C	With C	W/o C	With C
5	0.164	0.09204	0.01795	0.01181	0.4050	0.3034	0.1340	0.1087
7	0.1658	0.09162	0.01849	0.01202	0.4072	0.3027	0.1360	0.1096
10	0.167	0.09136	0.01789	0.01201	0.4087	0.3023	0.1338	0.1096
15	0.1735	0.09301	0.01861	0.01208	0.4165	0.3050	0.1364	0.1099
18	0.164	0.09045	0.01791	0.01192	0.4050	0.3007	0.1338	0.1092
20	0.167	0.09048	0.0181	0.01243	0.4087	0.3008	0.1345	0.1115
Average	0.166883	0.091493	0.018158	0.012045	0.408495	0.302475	0.134749	0.109746
Reduction (%)	45.18		33.67		25.95		18.55	
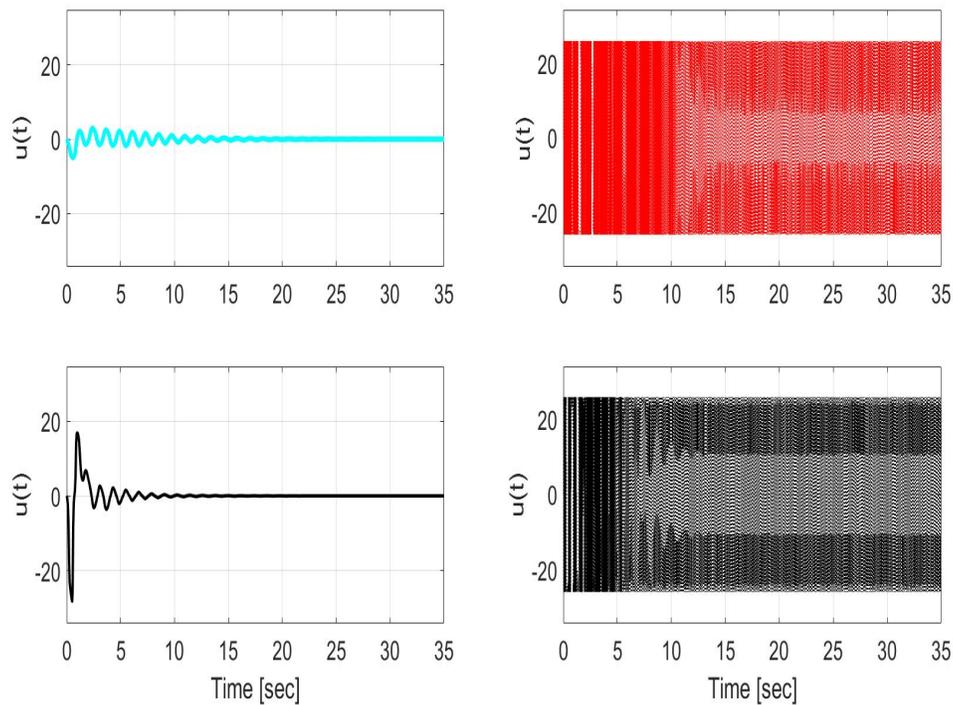
Figure 8. Control input used for LQR (**left**) and SMC (**right**) during closed-loop operation without (**top**) and with (**bottom**) uncertainty compensation. Note that the reduction of chattering is not the focus of the current result.

6.1.1. Various Initial Conditions

This section presents the performance improvement achieved using the proposed observer on the closed-loop LQR and SMC regulation control systems under four different sets of initial conditions. To illustrate the performance of the observer for different cases of initial conditions, Figures 9–12 show Monte Carlo-type results under 10 randomized iterations for the closed-loop LQR and SMC control systems, respectively, with and without the input uncertainty compensator in the observer. To summarize the results, bar graphs showing the average MSE are shown in Figure 13 and the corresponding MSE values are given in Table 5. These results further demonstrate the robustness of the proposed estimator under 10 randomized iterations of input-multiplicative parametric uncertainty.
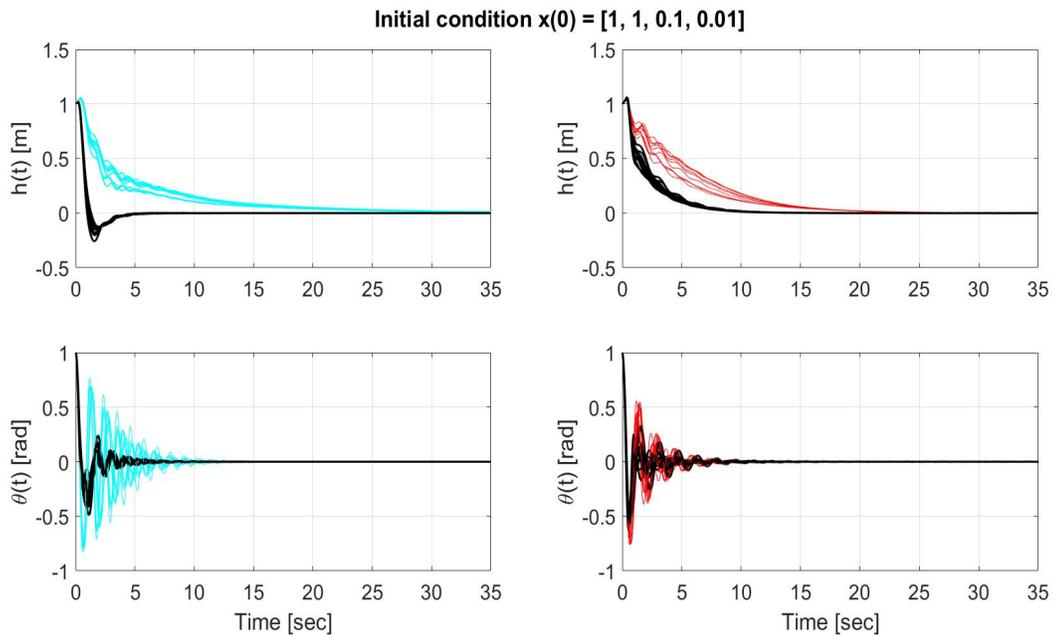
Figure 9. Time evolution of the states $h(t)$ (**top**) and $\theta(t)$ (**bottom**) for LQR without uncertainty compensation (left-cyan), LQR with uncertainty compensation (left-black), SMC without uncertainty compensation (right-red), SMC with uncertainty compensation (right-black) over the entire simulation time for initial condition x(0) = [1, 1, 0.1, 0.01].
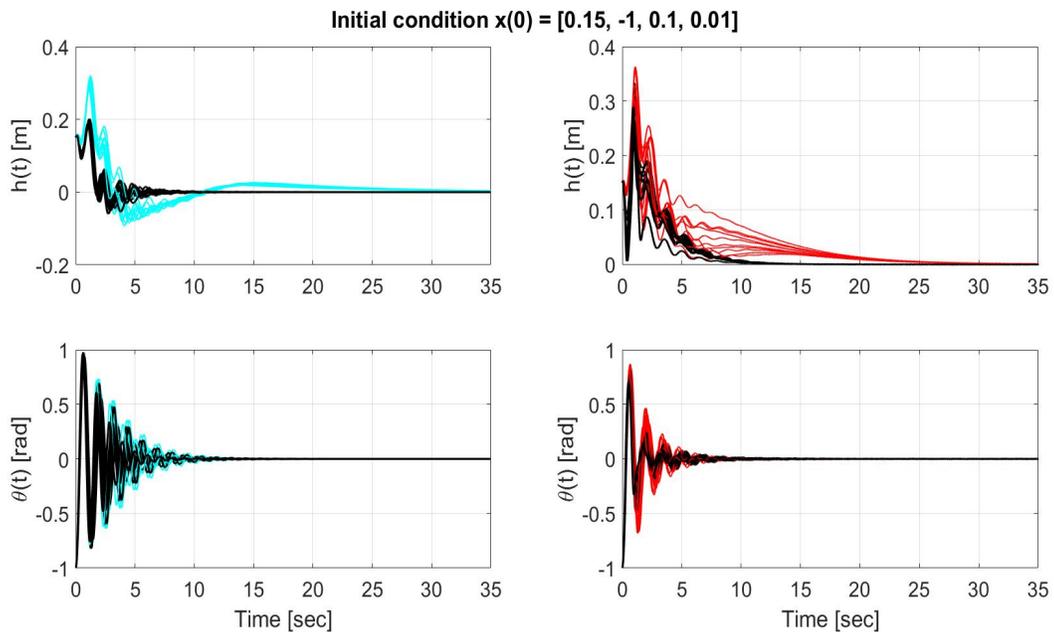

Figure 10. Time evolution of the states $h(t)$ (**top**) and $\theta(t)$ (**bottom**) for LQR without uncertainty compensation (left-cyan), LQR with uncertainty compensation (left-black), SMC without uncertainty compensation (right-red), SMC with uncertainty compensation (right-black) over the entire simulation time for initial condition x(0) = [0.15, −1, 0.1, 0.01].
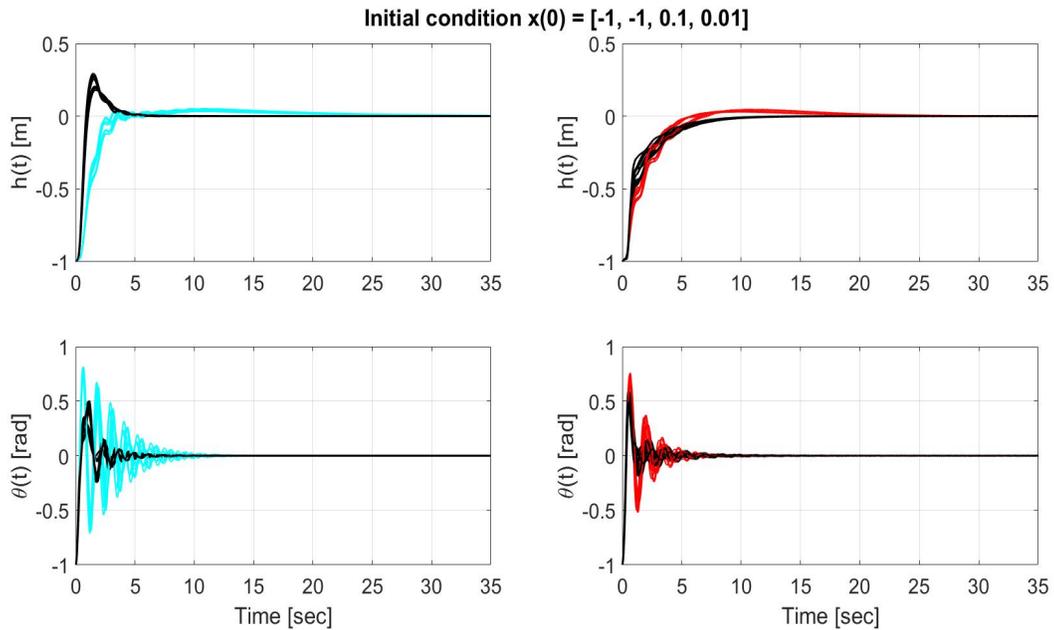
Figure 11. Time evolution of the states $h(t)$ (**top**) and $\theta(t)$ (**bottom**) for LQR without uncertainty compensation (left-cyan), LQR with uncertainty compensation (left-black), SMC without uncertainty compensation (right-red), SMC with uncertainty compensation (right-black) over the entire simulation time for initial condition x(0) = [$-1, -1, 0.1, 0.01$].
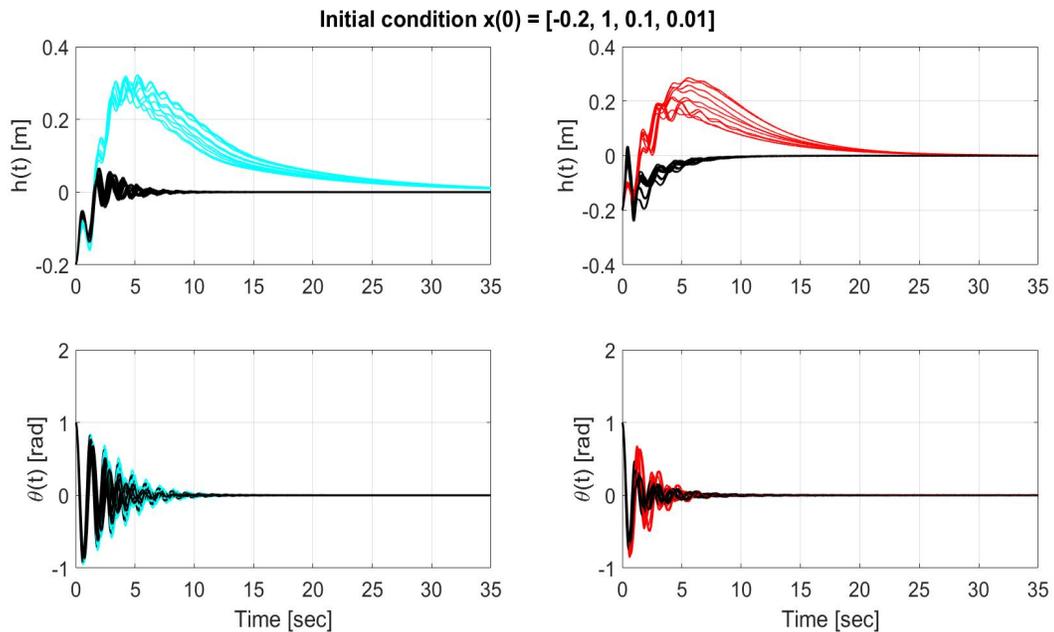

Figure 12. Time evolution of the states $h(t)$ (**top**) and $\theta(t)$ (**bottom**) for LQR without uncertainty compensation (left-cyan), LQR with uncertainty compensation (left-black), SMC without uncertainty compensation (right-red), SMC with uncertainty compensation (right-black) over the entire simulation time for initial condition x(0) = [$-0.2, 1, 0.1, 0.01$].
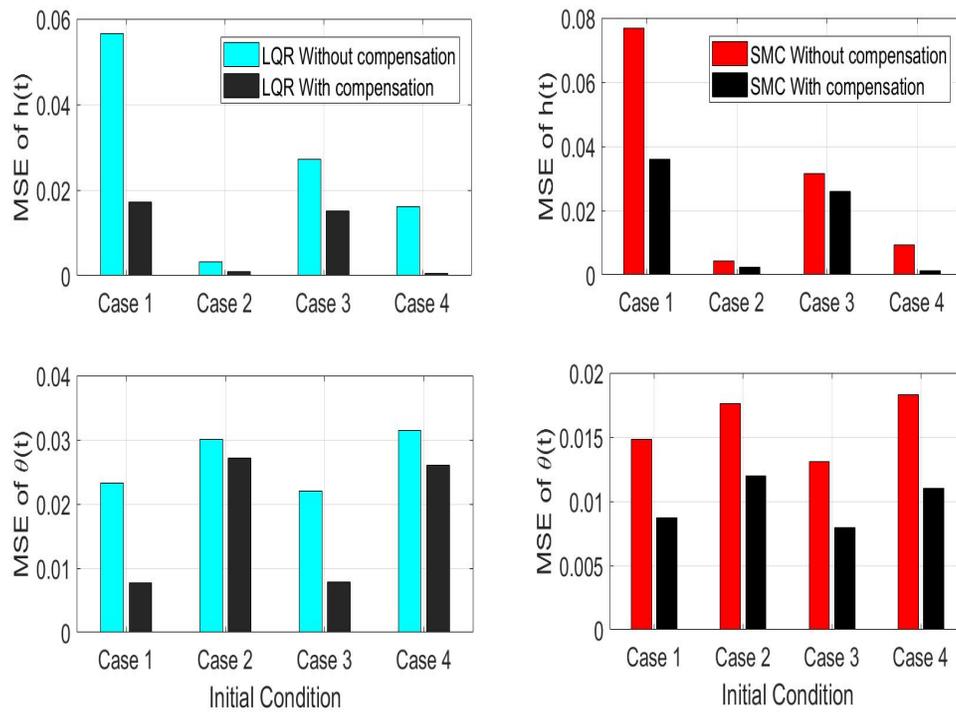
Figure 13. Mean squared error (MSE) during closed-loop operation for 10 iterations of 4 cases of initial conditions using LQR (**left**) and SMC (**right**) with and without uncertainty compensation.

Table 5. Mean squared error (MSE) during closed-loop operation for 10 iterations of randomized parameter uncertainty using LQR and SMC (Regulation) with uncertainty compensation (**With C**) and without uncertainty compensation (**W/o C**) for 4 different cases of initial conditions.

LQR REGULATION						
Initial Conditions	**MSE of $h(t)$**			**MSE of $\theta(t)$**		
	W/o C	**With C**	**Reduction %**	**W/o C**	**With C**	**Reduction %**
Case 1 x(0) = [1, 1, 0.1, 0.01]	0.05649	0.01711	69.71	0.02331	0.007758	66.72
Case 2 x(0) = [0.15, −1, 0.1, 0.01]	0.00316	0.001015	67.88	0.03001	0.02714	9.56
Case 3 x(0) = [−1, −1, 0.1, 0.01]	0.02721	0.01519	44.17	0.02195	0.007832	64.32
Case 4 x(0) = [−0.2, 1, 0.1, 0.01]	0.01622	0.0006201	96.18	0.03143	0.02609	16.99
Average	0.02577	0.0084838	69.49	0.026675	0.017205	39.40
SMC REGULATION						
Initial Conditions	**MSE of $h(t)$**			**MSE of $\theta(t)$**		
	W/o C	**With C**	**Reduction %**	**W/o C**	**With C**	**Reduction %**
Case 1 x(0) = [1, 1, 0.1, 0.01]	0.07693	0.03594	53.28	0.01481	0.008727	41.07
Case 2 x(0) = [0.15, −1, 0.1, 0.01]	0.004334	0.002419	44.19	0.0176	0.01196	32.05
Case 3 x(0) = [−1, −1, 0.1, 0.01]	0.03142	0.02597	17.35	0.01307	0.00794	39.25
Case 4 x(0) = [−0.2, 1, 0.1, 0.01]	0.009186	0.001317	85.66	0.01832	0.01099	40.01
Average	0.030468	0.0164115	50.12	0.01595	0.009904	38.10

6.2. Trajectory Tracking Control Using SMC

To further demonstrate the system performance, the proposed observer was tested in a trajectory tracking control objective using SMC. The SMC in the simulation is based on the design in Equations (49) and (50), where the control parameters were selected as summarized in Table 6. The desired trajectory was generated using the Matlab optimization function DYNOPT [41]. Specifically, the desired trajectory was defined as the minimum-energy trajectory that minimizes the cost function. The minimum-energy trajectory is used only as a proof-of-concept for tracking control.

$$J = \int_0^T \frac{1}{2}(M_c + m)x_3^2 + \frac{1}{2}ml^2 x_4^2 + mlx_3 x_4 \cos x_2 + mgl \cos x_2 dt \tag{53}$$

Table 6. Control gains.

$k_1 = 2$	$Z_0 = 26$
$k_2 = 5$	$\lambda = 30$
$k_3 = 5$	$\epsilon = 0.1460$
$k_4 = 1$	

Figure 14 shows the time evolution of the optimal trajectory and the states during closed-loop operation for the 10 iterations of randomized uncertainty. These results further demonstrate the improved performance that can be achieved using the proposed observer with input uncertainty compensation. Note that the focus of the current result is on the proof of finite time convergence for a sliding mode observer in the presence of input-multiplicative parametric uncertainty. To summarize the trajectory tracking results, Figure 15 shows a bar graph of the average MSE over six levels of parametric uncertainty and the corresponding MSE and RMS values are given in Table 7. Figure 16 shows the time evolution of the estimation error over the entire simulation time. Figure 17 shows the time evolution of the control input during closed-loop operation. Again, the chattering in SMC is not the focus here and is a subject of future work.

Table 7. Mean squared error (MSE) during closed-loop operation for 10 iterations of randomized parameter uncertainty using SMC (Tracking) with uncertainty compensation (**With C**) and without uncertainty compensation (**W/o C**).

|	SMC TRACKING							
Uncertainty	**MSE of $h(t)$**		**MSE of $\theta(t)$**		**RMS of $h(t)$**		**RMS of $\theta(t)$**	
(%)	**W/o C**	**With C**	**W/o C**	**With C**	**W/o C**	**With C**	**W/o C**	**With C**
5	0.1453	0.005788	0.02985	0.01963	0.3812	0.0761	0.1728	0.1401
7	0.1485	0.004584	0.02251	0.01976	0.3854	0.0677	0.1500	0.1406
10	0.1233	0.004682	0.03194	0.02003	0.3511	0.0684	0.1787	0.1415
15	0.1118	0.005419	0.03198	0.02311	0.3344	0.0736	0.1788	0.1520
18	0.1367	0.005004	0.02999	0.02135	0.3697	0.0707	0.1732	0.1461
20	0.192	0.01245	0.02757	0.02089	0.4382	0.1116	0.1660	0.1445
Average	0.142933	0.006321	0.028973	0.020795	0.376659	0.078024	0.169928	0.144146
Reduction (%)	95.58		28.23		79.29		15.17	
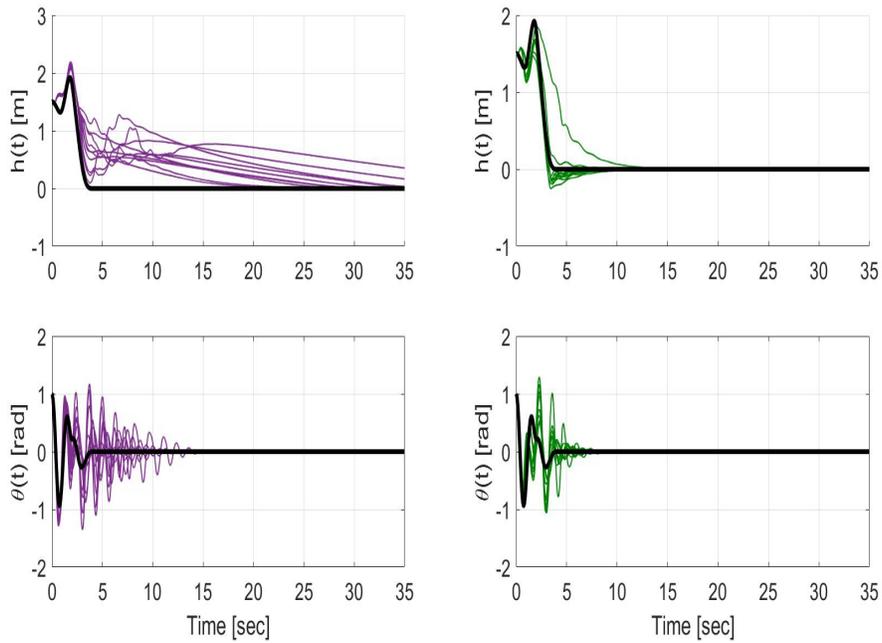
Figure 14. Time evolution of the optimal trajectory (black solid line) and the states $h(t)$ and $\theta(t)$ during closed-loop sliding mode controller operation for the cases without uncertainty compensation (**left-purple**) and with uncertainty compensation (**right-green**) in the observer design.
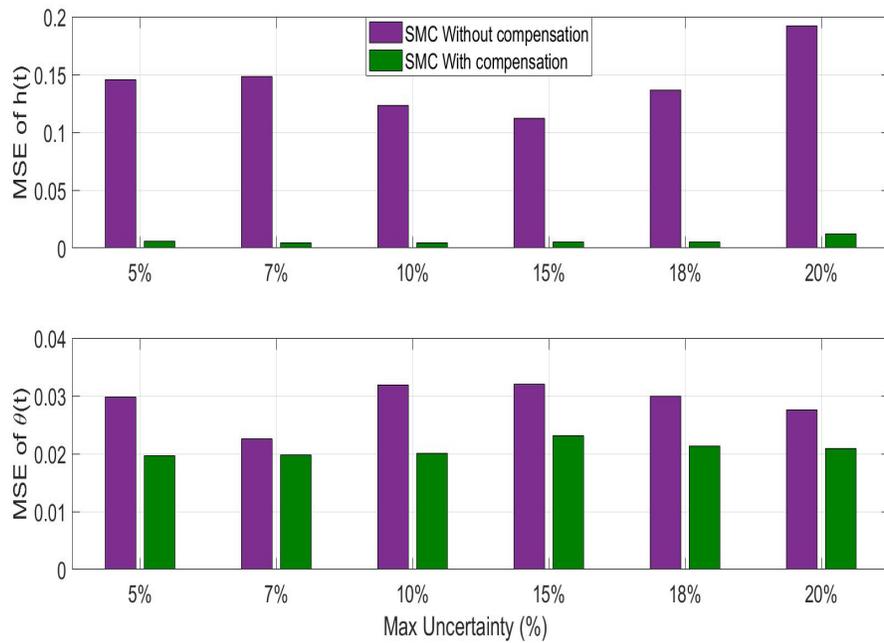

Figure 15. Average mean squared error (MSE) during closed-loop operation over 10 iterations of randomized parameter uncertainty using the sliding mode controller with and without uncertainty compensation.
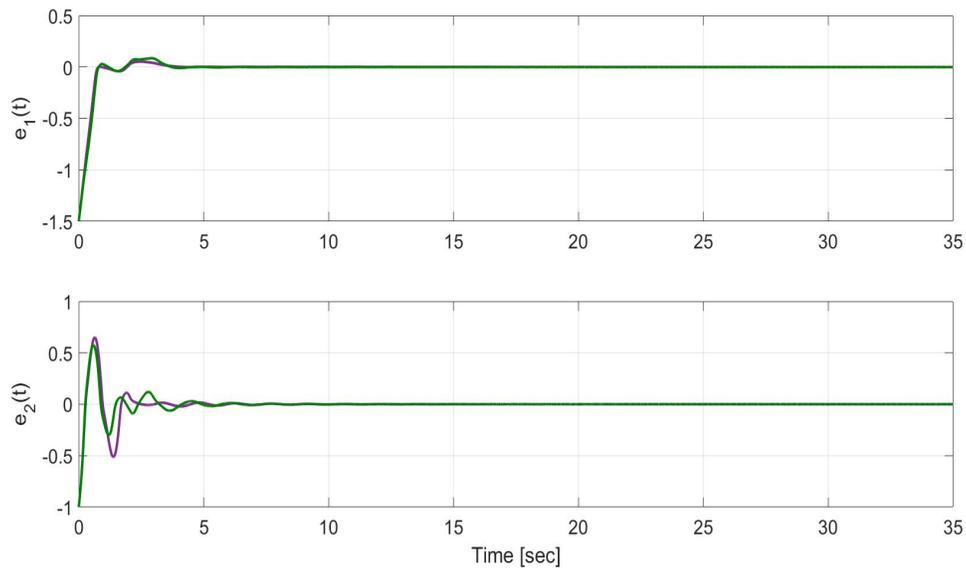
Figure 16. Time evolution of the estimation error in states $h(t)$ (**top**) and $\theta(t)$ (**bottom**) for SMC optimal trajectory tracking without uncertainty compensation (purple) and SMC optimal trajectory tracking with uncertainty compensation (green).
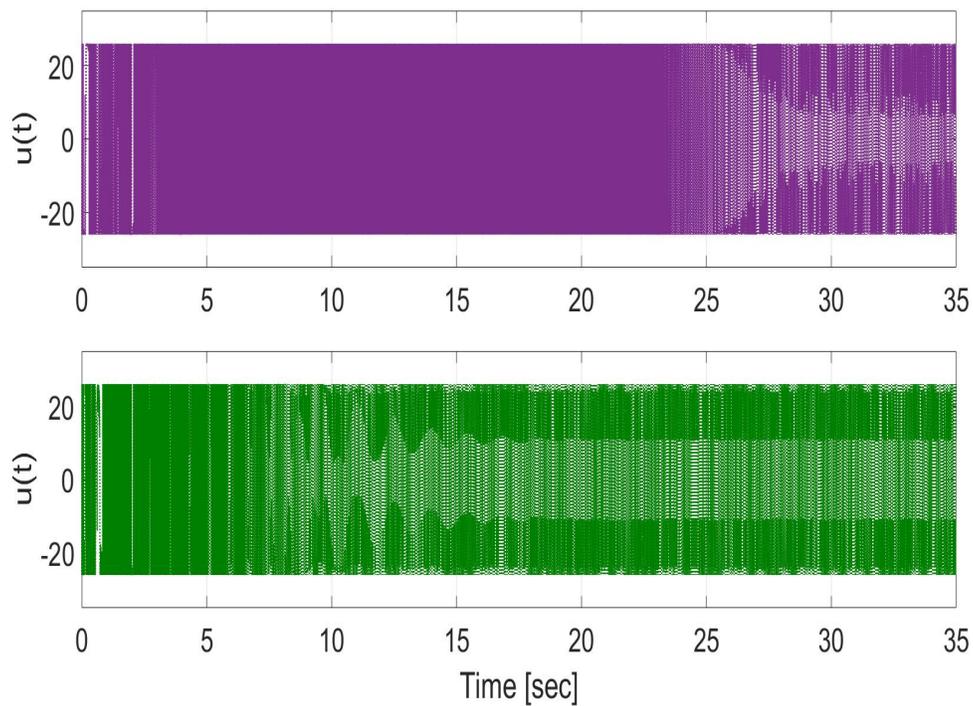

Figure 17. Control input used for SMC during closed-loop trajectory tracking control operation without (**top**) and with (**bottom**) uncertainty compensation. Note that the reduction of chattering is not the focus of the current result.

7. Conclusions

In this paper, a sliding mode observer is presented which achieves finite-time state estimation for a cart inverted pendulum in the presence of bounded disturbances and input-multiplicative parametric uncertainty. Key features of the result presented here are:

1. Rigorous proof of finite-time state estimation under input-multiplicative parametric uncertainty with detailed observer gain conditions.
2. A detailed simulation comparison study that illustrates the performance improvement that is achieved in using the input uncertainty compensation algorithm in the closed-loop system under six different levels of randomized uncertainty: 5%, 7%, 10%, 15%, 18%, 20%.
3. The percent reductions of MSE over the 10 iterations for each of the six levels of uncertainty are as follows:

    LQR Regulation shows 62.91% reduction in MSE of $h(t)$ and 31.94% reduction in MSE of $\theta(t)$ with the proposed estimator with uncertainty compensation.

    SMC Regulation shows 45.18% reduction in MSE of $h(t)$ and 33.67% reduction in MSE of $\theta(t)$ with the proposed estimator with uncertainty compensation.

    SMC Tracking shows 95.58% reduction in MSE of $h(t)$ and 28.23% reduction in MSE of $\theta(t)$ with the proposed estimator with uncertainty compensation.

    The numerical results clearly demonstrate the performance improvement that is achieved using the proposed uncertainty compensation technique in the observer.
4. The percent reductions of MSE over the 10 iterations for four different cases of initial conditions are as follows:

    LQR Regulation shows average reduction of 69.49 % in MSE of $h(t)$ and 39.40% in MSE of $\theta(t)$ with the proposed estimator with uncertainty compensation.

    SMC Regulation shows average reduction of 50.12 % in MSE of $h(t)$ and 38.10% in MSE of $\theta(t)$ with the proposed estimator with uncertainty compensation.

    The numerical results clearly demonstrate the performance improvement that is achieved using the proposed uncertainty compensation technique in the observer.
5. For completeness in analyzing the performance improvement using the input uncertainty compensator, the observer is applied to closed-loop systems using both SMC and LQR control methods.

In all of the simulated cases, a marked improvement is demonstrated by using the proposed estimator with uncertainty compensation.

Remark 8. *(Future Work) Future work will address a rigorous analysis of a practically implementable chatter-free nonlinear control method, which works in tandem with the sliding mode observer to compensate for input-multiplicative parametric uncertainty.*

Author Contributions: The individual contribution for this article were as follows: Conceptualization: A.K.J. and W.M. Methodology: A.K.J. Software : A.K.J. and K.B.K. Validation: A.K.J., W.M. and S.V.D. Formal analysis: A.K.J. and W.M. Investigation: A.K.J., W.M. and M.R. Visualization : A.K.J., K.B.K. and M.R. Resources: A.K.J. Writing Original Draft: A.K.J. Writing review and editing: A.K.J. Supervision: A.K.J., W.M. and S.V.D. Funding acquisition: W.M. All authors have read and agreed to the published version of the manuscript.

Conflicts of Interest: The authors declare no conflict of interest.

References

1. Al-Araji, A.S. An adaptive swing-up sliding mode controller design for a real inverted pendulum system based on Culture-Bees algorithm. *Eur. J. Control* **2019**, *45*, 45–56. [CrossRef]
2. Song, Y.; Du, D.; Sun, Q.; Zhou, H.; Fei, M. Sliding mode variable structure control for inverted pendulum visual servo systems. *IFAC-PapersOnLine* **2019**, *52*, 262–267. [CrossRef]
3. Irfan, S.; Mehmood, A.; Razzaq, M.T.; Iqbal, J. Advanced sliding mode control techniques for inverted pendulum: Modelling and simulation. *Eng. Sci. Technol. Int. J.* **2018**, *21*, 753–759. [CrossRef]
4. Ata, B.; Coban, R. Decoupled Backstepping Sliding Mode Control of Underactuated Systems with Uncertainty: Experimental Results. *Arab. J. Sci. Eng.* **2019**, *44*, 7013–7021. [CrossRef]
5. Ullah, S.; Khan, Q.; Mehmood, A.; Bhatti, A.I. Robust Backstepping Sliding Mode Control Design for a Class of Underactuated Electro-Mechanical Nonlinear Systems. *J. Electr. Eng. Technol.* **2020**, *15*, 1821–1828. [CrossRef]
6. Ovalle, L.; Ríos, H.; Llama, M. Robust output-feedback control for the cart–pole system: A coupled super-twisting sliding-mode approach. *IET Control Theory Appl.* **2019**, *13*, 269–278. [CrossRef]
7. Mobayen, S. Adaptive global sliding mode control of underactuated systems using a super-twisting scheme: An experimental study. *J. Vib. Control* **2019**, *25*, 2215–2224. [CrossRef]
8. Zhang, M.; Huang, J.; Chen, F. Super twisting control algorithm for Velocity Control of Mobile Wheeled Inverted Pendulum Systems. In Proceedings of the 2018 IEEE Workshop on Advanced Robotics and its Social Impacts (ARSO), Genova, Italy, 27–28 September 2018; pp. 3–8.
9. Chalanga, A.; Patil, M.; Bandyopadhyay, B.; Arya, H. Output regulation using new sliding surface with an implementation on inverted pendulum system. *Eur. J. Control* **2019**, *45*, 85–91. [CrossRef]
10. Hanwate, S.; Hote, Y.V.; Budhraja, A. Design and implementation of adaptive control logic for cart-inverted pendulum system. *Proc. Inst. Mech. Eng. Part I J. Syst. Control. Eng.* **2019**, *233*, 164–178. [CrossRef]
11. Gandarilla, I.; Santibañez, V.; Sandoval, J. Control of a self-balancing robot with two degrees of freedom via IDA-PBC. *ISA Trans.* **2019**, *88*, 102–112. [CrossRef]
12. Kennedy, E.; King, E.; Tran, H. Real-time implementation and analysis of a modified energy based controller for the swing-up of an inverted pendulum on a cart. *Eur. J. Control* **2019**, *50*, 176–187. [CrossRef]
13. Nath, K.; Dewan, L. A comparative analysis of linear quadratic regulator and sliding mode control for a rotary inverted pendulum. In Proceedings of the 2018 International Conference on Recent Trends in Electrical, Control and Communication (RTECC), Chennai, India, 20–22 March 2018; pp. 302–307.
14. Hanwate, S.; Hote, Y.V. Relative stability analysis of perturbed cart inverted pendulum: An experimental approach. *IETE Tech. Rev.* **2018**, *35*, 640–655. [CrossRef]
15. Liu, P.; Yu, H.; Cang, S. Adaptive neural network tracking control for underactuated systems with matched and mismatched disturbances. *Nonlinear Dyn.* **2019**, *98*, 1447–1464. [CrossRef]
16. Xia, X.; Xia, J.; Gang, M.; Zhang, Q.; Wang, J. Discrete Dynamics-Based Parameter Analysis and Optimization of Fuzzy Controller for Inverted Pendulum Systems Based on Chaos Algorithm. *Discret. Dyn. Nat. Soc.* **2020**, *2020*, 3639508.
17. Al-Mekhlafi, M.A.; Wahid, H.; Aziz, A.A. Adaptive Neuro-Fuzzy Control Approach for a Single Inverted Pendulum System. *Int. J. Electr. Comput. Eng.* **2018**, *8* , 3657 3665. [CrossRef]
18. Guesmi, K.; Bdirina, E.K. Model Predictive Control by Change Control Rate Maximization and Control Action Minimization. *Electroteh. Electron. Autom.* **2019**, *67*, 68–75.
19. Sambo, A.; Bala, F.S.; Tahir, N.M.; Babawuro, A. Optimal control of inverted pendulum on cart system. *J. Phys. Conf. Ser. Iop Publ.* **2020**, *1502*, 012024. [CrossRef]
20. Bucolo, M., Buscarino, A., Famoso, C., Fortuna, L., Frasca, M. Control of imperfect dynamical systems. *Nonlinear Dyn.* **2019**, *98*, 2989–2999. [CrossRef]
21. Mahmoud, M.S.; Nasir, M.T. Robust control design of wheeled inverted pendulum assistant robot. *IEEE/CAA J. Autom. Sin.* **2017**, *4*, 628–638. [CrossRef]

22. Bakarx, P.; Klaux, M.; Fikar, M. Comparison of inverted pendulum stabilization with PID, LQ, and MPC control. In Proceedings of the 2018 Cybernetics & Informatics (K & I), Lazy pod Makytou, Slovakia, 31 January–3 February 2018; pp. 1–6.
23. Peker, F.; Kaya, I. Identification and real time control of an inverted pendulum using PI-PD controller. In Proceedings of the 2017 21st International Conference on System Theory, Control and Computing (ICSTCC), Sinaia, Romania, 19–21 October 2017; pp. 771–776.
24. Chen, C.; Zhao, D.; Qiu, L. Control of an Under-Sensed and Under-Actuated Linear Inverted Pendulum. In Proceedings of the 2018 57th Annual Conference of the Society of Instrument and Control Engineers of Japan (SICE), Nara, Japan, 11–14 September 2018; pp. 1301–1306.
25. Howimanporn, S.; Thanok, S.; Chookaew, S.; Sootkaneung, W. Design and implementation of PSO based LQR control for inverted pendulum through PLC. In Proceedings of the 2016 IEEE/SICE International Symposium on System Integration (SII), Sapporo, Japan, 13–15 December 2016; pp. 664–669.
26. Basin, M.V.; Rodriguez-Ramirez, P.C.; Ding, S.X.; Daszenies, T.; Shtessel, Y.B. Continuous fixed-time control for cart inverted pendulum stabilization. In Proceedings of the 2016 IEEE 55th Conference on Decision and Control (CDC), Las Vegas, NV, USA, 12–14 December 2016; pp. 6440–6445.
27. Chaoui, H.; Yadav, S. Adaptive motion and posture control of inverted pendulums with nonlinear friction compensation. In Proceedings of the 2016 IEEE 25th International Symposium on Industrial Electronics (ISIE), Santa Clara, CA, USA, 8–10 June 2016; pp. 344–349.
28. Estupiñán, E.; Arévalo, J.; Cano, D.; Parra, O. Performance evaluation of inverted pendulum control: Linear and nonlinear techniques. In Proceedings of the 2017 IEEE 3rd Colombian Conference on Automatic Control (CCAC), Cartagena, Colombia, 18–20 October 2017; pp. 1–7.
29. Coban, R.; Ata, B. Decoupled sliding mode control of an inverted pendulum on a cart: An experimental study. In Proceedings of the 2017 IEEE International Conference on Advanced Intelligent Mechatronics (AIM), Munich, Germany, 3–7 July 2017; pp. 993–997.
30. Huang, J.; Ri, S.; Liu, L.; Wang, Y.; Kim, J.; Pak, G. Nonlinear disturbance observer-based dynamic surface control of mobile wheeled inverted pendulum. *IEEE Trans. Control. Syst. Technol.* **2015**, *23*, 2400–2407. [CrossRef]
31. Silik, Y.; Yaman, U. Control of Rotary Inverted Pendulum by Using On–Off Type of Cold Gas Thrusters. *Actuators* **2020**, *9*, 95. [CrossRef]
32. Ning, Y.; Yue, M.; Lin, Z. Time-Optimal Control of Underactuated Wheeled Inverted Pendulum Vehicles Along Specified Paths. In Proceedings of the 2020 IEEE 5th International Conference on Advanced Robotics and Mechatronics (ICARM), Shenzhen, China, 18–21 December 2020; pp. 694–699.
33. Scalera, L.; Gasparetto, A.; Zanotto, D. Design and experimental validation of a 3-dof underactuated pendulum-like robot. *IEEE/ASME Trans. Mechatronics* **2019**, *25*, 217–228. [CrossRef]
34. Mehedi, I.M.; Ansari, U.; Bajodah, A.H.; AL-Saggaf, U.M.; Kada, B.; Rawa, M.J. Underactuated rotary inverted pendulum control using robust generalized dynamic inversion. *J. Vib. Control* **2020**. [CrossRef]
35. Huang, J.; Zhang, M.; Ri, S.; Xiong, C.; Li, Z.; Kang, Y. High-order disturbance-observer-based sliding mode control for mobile wheeled inverted pendulum systems. *IEEE Trans. Ind. Electron.* **2019**, *67*, 2030–2041. [CrossRef]
36. Friedland, B. *Control System Design: An Introduction to State-Space Methods*; Courier Corporation: North Chelmsford, MA, USA, 2012.
37. Kidambi, K.B.; Ramos-Pedroza, N.; MacKunis, W.; Drakunov, S.V. A closed-loop nonlinear control and sliding mode estimation strategy for fluid flow regulation. *Int. J. Robust Nonlinear Control* **2019**, *29*, 779–792. [CrossRef]
38. Drakunov, S.V. Sliding-mode observers based on equivalent control method. In Proceedings of the 31st IEEE Conference on Decision and Control, Tucson, AZ, USA, 16–18 December 1992; pp. 2368–2369.
39. Kidambi, K.B.; MacKunis, W.; Drakunov, S.V.; Golubev, V. A sliding mode estimation method for fluid flow fields using a differential inclusions-based analysis. *Int. J. Control* **2020**, 1–10. [CrossRef]

40. Drakunov, S.V. Sliding mode control with multiple equilibrium manifolds. *J. Dyn. Syst. Meas. Control* **1994**, *55*, 101–108.

41. Cizniar, M.; Fikar, M.; Latifi, M. *Matlab Dynamic Optimisation Code Dynopt. User'S Guide*; KIRP FCHPT STU: Bratislava, Slovakia, 2006.

Publisher's Note: MDPI stays neutral with regard to jurisdictional claims in published maps and institutional affiliations.